HAL open science

Replenishment of Near-Surface Water Ice by Impacts Into Ceres' Volatile-Rich Crust: Observations by Dawn's Gamma Ray and Neutron Detector

T. H. Prettyman, N. Yamashita, M. E. Landis, J. C. Castillo-Rogez, N. Schörghofer, C. M. Pieters, H. G. Sizemore, H. Hiesinger, S. Marchi, H. Y. Mcsween, et al.

To cite this version:

T. H. Prettyman, N. Yamashita, M. E. Landis, J. C. Castillo-Rogez, N. Schörghofer, et al.. Replenishment of Near-Surface Water Ice by Impacts Into Ceres' Volatile-Rich Crust: Observations by Dawn's Gamma Ray and Neutron Detector. Geophysical Research Letters, 2021, 48, 10.1029/2021GL094223 . insu-03672409

HAL Id: insu-03672409

https://insu.hal.science/insu-03672409

Submitted on 19 May 2022

HAL is a multi-disciplinary open access archive for the deposit and dissemination of scientific research documents, whether they are published or not. The documents may come from teaching and research institutions in France or abroad, or from public or private research centers.

L'archive ouverte pluridisciplinaire **HAL**, est destinée au dépôt et à la diffusion de documents scientifiques de niveau recherche, publiés ou non, émanant des établissements d'enseignement et de recherche français ou étrangers, des laboratoires publics ou privés.

Distributed under a Creative Commons Attribution 4.0 International License

Check for updates

ADVANCING EARTH AND SPACE SCIENCE

Geophysical Research Letters

RESEARCH LETTER
10.1029/2021GL094223

Key Points:

- Neutron spectroscopy reveals enhanced hydrogen concentrations in the outermost meter of the surface of a prominent young, complex crater
- Results confirm Ceres outer crust is ice rich and support retention of water ice within impact ejecta on airless, icy bodies
- The data imply partial control of regolith ice content by large impacts, relaxing constraints on surface age and regolith grain size

Supporting Information:

Supporting Information may be found in the online version of this article.

Correspondence to:

T. H. Prettyman,
prettyman@psi.edu

Citation:

Prettyman, T. H., Yamashita, N., Landis, M. E., Castillo-Rogez, J. C., Schörghofer, N., Pieters, C. M., et al. (2021). Replenishment of near-surface water ice by impacts into Ceres' volatile-rich crust: Observations by Dawn's Gamma Ray and Neutron Detector. *Geophysical Research Letters*, *48*, e2021GL094223. https://doi.org/10.1029/2021GL094223

Received 25 MAY 2021
Accepted 9 JUL 2021

© 2021. The Authors.
This is an open access article under the terms of the Creative Commons Attribution License, which permits use, distribution and reproduction in any medium, provided the original work is properly cited.

Replenishment of Near-Surface Water Ice by Impacts Into Ceres' Volatile-Rich Crust: Observations by Dawn's Gamma Ray and Neutron Detector

T. H. Prettyman[1], N. Yamashita[1], M. E. Landis[2], J. C. Castillo-Rogez[3], N. Schörghofer[1], C. M. Pieters[1,4], H. G. Sizemore[1], H. Hiesinger[5], S. Marchi[6], H. Y. McSween[7], R. S. Park[3], M. J. Toplis[8], C. A. Raymond[3], and C. T. Russell[9]

[1]Planetary Science Institute, Tucson, AZ, USA, [2]Laboratory for Atmospheric and Space Physics, University of Colorado, Boulder, CO, USA, [3]Jet Propulsion Laboratory, California Institute of Technology, Pasadena, CA, USA, [4]Brown University, Providence, RI, USA, [5]Institut für Planetologie, Westfälische Wilhelms-Universität Münster, Münster, Germany, [6]Southwest Research Institute, Boulder, CO, USA, [7]University of Tennessee, Knoxville, TN, USA, [8]L'Institut de Recherche en Astrophysique et Planétologie (University of Toulouse, UT3, CNRS), Toulouse, France, [9]University of California Los Angeles, Los Angeles, CA, USA

Abstract Ceres' regolith contains water ice that has receded in response to insolation-driven sublimation. Specially targeted, high spatial-resolution measurements of hydrogen by Dawn's Gamma Ray and Neutron Detector (GRaND) reveal elevated hydrogen concentrations in and around Occator, a young, 90 km diameter, complex crater located at 19.82°N where near-surface ice is not expected. The excess hydrogen can be explained by impact excavation of water-rich outer crustal materials and their emplacement in the crater floor and ejecta blanket. This is supported by thermophysical models that show water ice could survive at sub-meter depths, given Occator's relatively young age (~20 Myr). We hypothesize that the regolith can be replenished with ice from large impacts and that this process partially controls the distribution and depth of near surface ice. This is supported by results from Occator and similarities in the global distribution of hydrogen and the pattern of large craters (20–100 km diameter).

Plain Language Summary The outermost meter of dwarf planet Ceres contains water ice that is gradually sublimating in response to heating of the surface by sunlight. Since Ceres' axis of rotation is nearly perpendicular to the Sun's rays, ice has receded to greater depths at the equator than the poles. The distribution of subsurface ice within this outer layer was inferred from measurements of hydrogen by Dawn's Gamma Ray and Neutron Detector. Special operations during Dawn's last mission phase brought the spacecraft close to the surface, enabling measurements within and around a large, young crater called Occator. Anomalously high concentrations of hydrogen were detected, suggesting the impact that formed Occator excavated water rich materials from the crust and deposited them on the surface. Comparison of the global distribution of hydrogen with the pattern of large craters on Ceres further supports excavation of crustal ice by impacts as a partial control on the depth of ice near the surface. Results confirm that Ceres' crust is rich in water ice and show that ice can survive in materials ejected by impacts into airless, icy bodies.

1. Introduction

The dwarf planet Ceres, the largest body in the main asteroid belt (469.7 km volumetric mean radius), is water-rich (Russell et al., 2016). As Ceres evolved, liquid water interacted with rock within the interior to produce hydrated minerals (McSween et al., 2017). Ceres' average interior structure consists of a rocky mantle and a ~40 km thick crust, dominated by the frozen remnants of an ancient, global ocean (Castillo-Rogez et al., 2018; Ermakov et al., 2017). Rheological constraints indicate that the crust is volatile-rich, containing water ice, phyllosilicates, salts, and possibly clathrate hydrates (Fu et al., 2017). Residual brines at the base of the crust could be a source for active cryomagmatism (e.g., Quick et al., 2019; Raymond et al., 2020; Ruesch et al., 2019). High-resolution gravity data imply a positive density gradient in Ceres' crust, interpreted as enrichment of dense oceanic precipitates in the lower part of the crust in contrast to a volatile-rich outer crust (Park et al., 2020).

The ice content of different crustal layers can be inferred from diverse remote-sensing data sets, including nuclear spectroscopy, geomorphology, and gravity. Surficial water ice has been detected within some mid-to-high latitude craters (Combe et al., 2019) and the presence of complex craters with fluidized ejecta, lobate flow features, and pitted terrain indicate water ice is abundant within the few km depths probed by impacts (e.g., Sizemore et al., 2017, 2019). Gamma Ray and Neutron Detector (GRaND) measurements reveal the presence of a global ice table within a few millimeters of the surface at the poles that has receded to greater depths at lower latitudes due to increased solar insolation, consistent with Ceres' obliquity history (Prettyman et al., 2017).

Previous analyses of GRaND data support 20 vol.% water ice in the near-surface ice table, with ice below the depth of sensitivity (a few decimeters) near the equator; whereas, the bulk crustal average water content is inferred to be >60 vol.% based on geophysical measurements of crustal density and strength (Fu et al., 2017; Park et al., 2020). Impact processes are key to understanding the connection between the volatile-rich crustal reservoir and the regolith. A simple-to-complex transition occurs for craters with diameters greater than about 10 km (Hiesinger et al., 2016; Schenk et al., 2021). Furthermore, impacts that formed large craters exposed crustal materials from a wide range of depths within the outer crust, with the excavation depth roughly 10% of the crater diameter (Marchi et al., 2016). As such, large impacts have the potential to redistribute ice within the outer crust.

We use hydrogen mapping data acquired by Dawn's GRaND to investigate the effect of impacts on shallow-regolith water ice content. We hypothesize that impacts can bring water ice from the outer crust to the surface, replenishing the regolith with ice. As such, the distribution of near surface water ice in the upper few decimeters of the regolith as sensed by GRaND is shaped both by large impacts and long-term insolation-driven sublimation. We test this hypothesis with high-spatial-resolution GRaND data acquired in Dawn's final mission phase. The high-resolution data are sensitive to the composition of the interior and ejecta blanket of the young, complex crater Occator. Lower-resolution data acquired by GRaND during Dawn's primary mission enable investigations of the global relationships between cratering and regolith hydrogen content.

2. Hydrogen Mapping With High Spatial Resolution GRaND Data

In Dawn's final mission phase, the spacecraft maneuvered into a highly eccentric orbit with low periapsis (30–50 km, Figures 1a and 1b and Text S1). This enabled acquisition of high-spatial-resolution GRaND data, on scales comparable to geologic units over a wide range of latitudes in both the eastern and western hemispheres. Analyses of high-resolution data can be compared with the elemental measurements determined from GRaND data acquired in Dawn's primary mission from a low altitude mapping orbit (LAMO) with 385 km mean altitude (Prettyman et al., 2017). Since spatial resolution scales with altitude (Prettyman et al., 2019), the eccentric orbits achieved up to 10X improvement in spatial resolution compared to LAMO.

A primary target of the eccentric orbits was Occator crater, a very young (<20 Myr) (Neesemann et al., 2019) 90 km diameter, complex crater located at about 19.82°N and 239.33°E within Hanami Planum. The crater contains prominent faculae as well as lobate deposits and fluidized ejecta, which likely contain water ice (Scully et al., 2019). Thus, the geomorphology supports impact into an ice-rich substrate. The crater and immediate surroundings were well sampled with multiple orbits with periapsides near 35 km altitude, corresponding to an intrinsic spatial resolution of about 50 km full-width-at-half-maximum for GRaND. This allowed measurements of hydrogen within the crater interior and portions of the ejecta blanket, providing constraints on processes underlying crater formation and the fate of hydrogen-bearing materials.

The concentration of hydrogen was determined from the leakage flux of low-energy neutrons produced by the interaction of galactic cosmic rays (GCRs) with Ceres' regolith. Measurements of the ^{6}Li(n,α) reaction rate with GRaND's + Z lithium-loaded glass (LiG) scintillator (Prettyman et al., 2011) provide a high-intensity signal from which the concentration of hydrogen can be determined with high precision and accuracy (Figure 1c) (Prettyman et al., 2017). This signal was used to map hydrogen on fine spatial scales, 50–150 km, using data acquired below 100 km altitude.

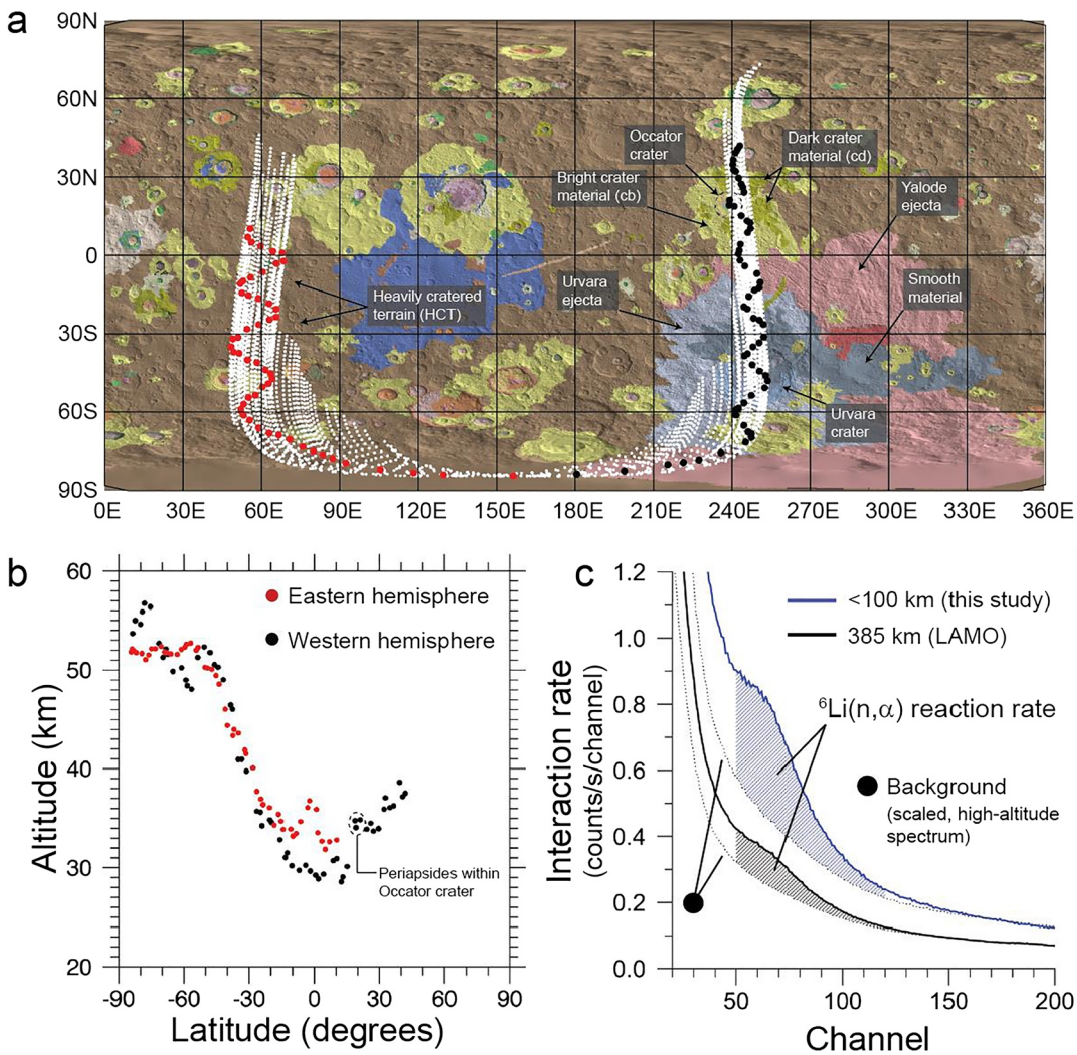

Figure 1. Close-proximity measurements. (a) Highly eccentric orbits (south-north trajectory) enabled the acquisition of Gamma Ray and Neutron Detector (GRaND) data with 35 s accumulation intervals at over 5,000 locations with altitudes less than 100 km (white points). Circles (red and black) indicate the measurement locations closest to the periapsides of the 113 orbits used in the analysis (Text S1). The measurements sampled geologic units in the eastern and western hemispheres along the 60°E and 240°E meridian, including the ~20 Myr old Occator crater (Neesemann et al., 2019), centered at 239.33°E and 19.82°N, and its ejecta blanket. See Williams et al. (2019) for geological unit definitions. (b) Altitudes of periapsis less than 30 km were achieved at some locations near the equator, with higher altitudes toward the poles. (c) Close proximity enabled acquisition of neutron counting data with high spatial resolution and precision. The ^{6}Li(n,α) reaction rate in GRaND's lithium-loaded glass (LiG) scintillator (shaded areas) is sensitive to regolith hydrogen content (Text S1). The average reaction rate below 100 km was about 3X higher than observed in Dawn's low altitude mapping orbit (LAMO).

Texts S1 and S2 describe the data reduction and mapping methods. The ^{6}Li(n,α) reaction rate at each orbital location was determined and corrected for variations in the flux of GCRs using data acquired near the apoapsis of each orbit. Corrections for measurement geometry were made using the forward model described by Prettyman et al. (2017) that accounts for Ceres' overall shape and local topography when the spacecraft was in close proximity to the surface. The corrected counting data were mapped onto the surface using a circle superposition algorithm that accounts for variations in the resolution of the spectrometer with altitude. High-resolution maps are shown in Figure 2.

To validate the sensitivity of the elliptical data to the interior of Occator crater, we averaged the ^{6}Li(n,α) counts for three nearly identical orbits with periapsides near the center of the crater (Figure S1). The data

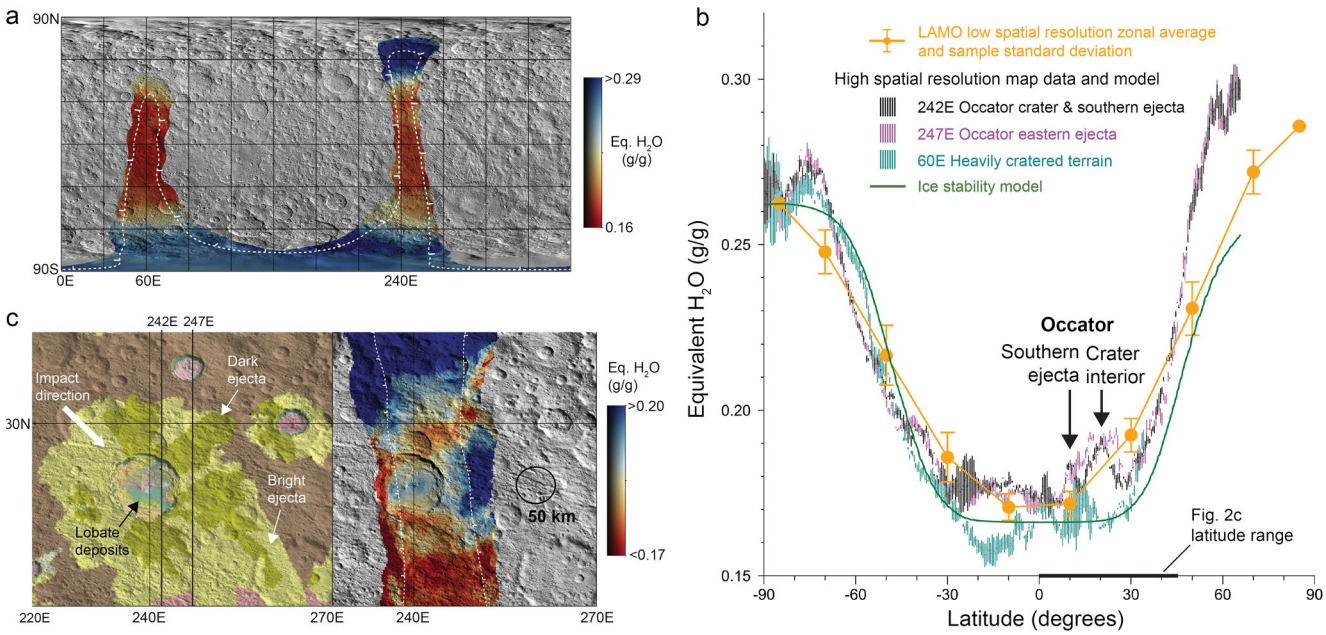

Figure 2. Distribution of subsurface hydrogen. (a) The equirectangular map of water-equivalent hydrogen, was determined from ^{6}Li(n,α) reaction rates measured below 100 km altitude. The white contour line, which approximates the boundary of the point cloud in Figure 1a, delineates the most highly sampled region, with contributions from >50 measurements at each map location. Outside the point cloud, hydrogen concentrations are extrapolated from the data. (b) The distribution of hydrogen in (a) is plotted for selected meridians. The population standard deviation in hydrogen concentration, determined by Monte Carlo error propagation, is represented by vertical lines. The distribution of hydrogen, which is more variable than the low altitude mapping orbit (LAMO) zonal average (Prettyman et al., 2017) is consistent with a globally receding ice table. The mapping algorithm was applied to simulated, high-resolution neutron measurements of the distribution of ice determined by an ice stability model, assuming ice-cemented soil with 1 μm grain size, 0.2 porosity, and 10 wt.% water ice (Prettyman et al., 2017). These parameters produced a close match to the neutron counting data acquired in LAMO. (c) The low-altitude data reveal elevated concentrations of hydrogen in and around Occator crater. Map variations on spatial scales greater than 50 km (black circle) can be interpreted as changes in subsurface composition. A geologic map of the Occator region is provided for context (Scully et al., 2019; Williams et al., 2018, with units defined therein). Map data are superimposed on shaded relief.

reveal a significant suppression of counts within the crater and to the south of the crater, consistent with mapped enhancements in hydrogen shown in Figure 2b. Furthermore, simulations of the response of GRaND to neutrons emitted within geologic units (Figure S1) supports the sensitivity of the measurements to ice in the lobate deposits and terrace material inside the crater as well as ice in the ejecta blanket.

3. Results

The high spatial resolution maps reveal similar large-scale trends as observed in LAMO (Prettyman et al., 2017) with more hydrogen at high latitudes than near the equator (Figures 2a and 2b). This pattern is consistent with the presence of a receding ice table. If the regolith initially contained ice-cemented soil, then the LAMO data can be explained by a low-diffusivity regolith with about 0.2 porosity and 1 μm grain size (Prettyman et al., 2017). In this case, ice is expected to have receded to about 80–90 cm at the equator over Ceres' lifetime. Ice would have been preserved at submillimeter depths poleward of 60° latitude in the northern and southern hemispheres.

Forward modeling was used to determine the concentration of hydrogen that would have been observed by GRaND from the eccentric orbit given the distribution of ice that best fits the LAMO data per Prettyman et al. (2017) (green curve in Figure 2b). The modeled variation in bulk regolith hydrogen approximates the observed variation in the high-resolution data at southern high latitudes. Near the equator (±30° latitude), the model is nearly constant, indicating ice in this region at depths greater than sensed by GRaND. Within this region, the "best fit" model ice depths from Prettyman et al. (2017) ranged from 50 to 90 cm.

In contrast to the model, the high-resolution measurements show variations in hydrogen content with latitude and longitude in the equatorial band. For example, the concentration of hydrogen at low latitudes in

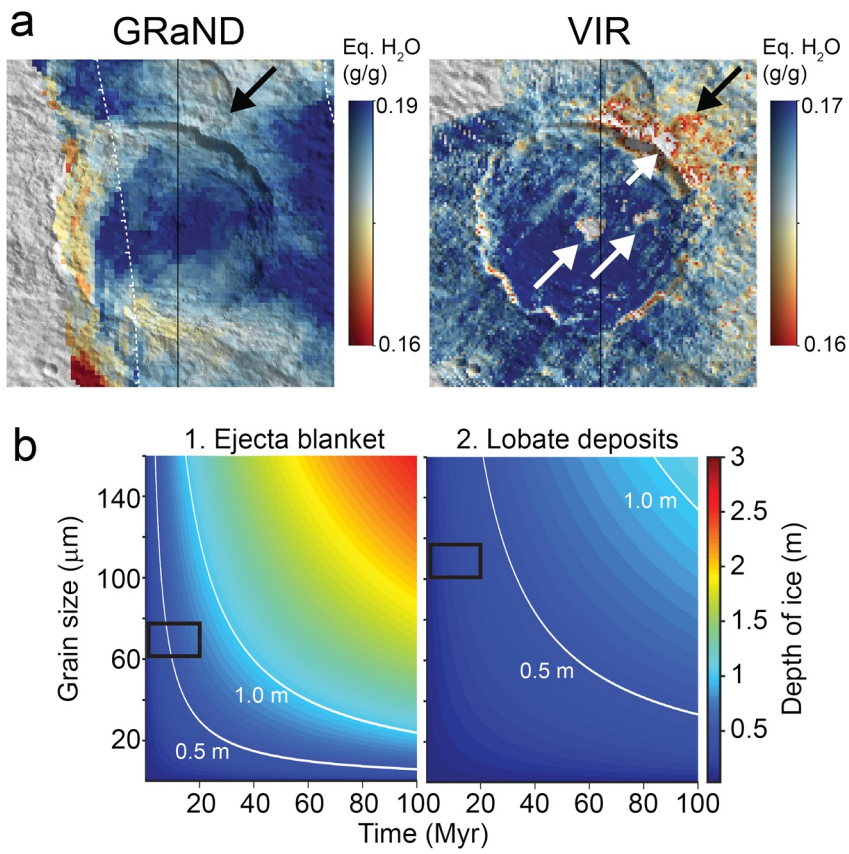

Figure 3. Evidence for water ice at Occator crater. (a) The distribution of hydrogen within and immediately surrounding Occator determined by the Gamma Ray and Neutron Detector (GRaND) is compared to that inferred from VIR mineralogy (Text S3) (Marchi et al., 2019; Raponi et al., 2019). The VIR-derived hydrogen concentration within the facula and portions of the crater rim is <16 wt.% eq. H_2O (white arrows point to regions with no data in the range indicated by the scalebar). The faculae are smaller than can be resolved by GRaND. Both maps include a lobe of relatively hydrogen-poor material extending from the north and east of the crater (black arrows). (b) Thermophysical modeling shows that ice could survive at depths sensed by GRaND for a range of reported ages (Neesemann et al., 2019) and feasible regolith thermophysical properties (porosity and grain size). Two cases are modeled: 1. Impact ejecta emplaced outside the crater are assumed to have the same porosity (0.2) as determined by GRaND in LAMO. 2. Within the interior of the crater, ice may have been concentrated in lobate deposits during crater formation (Scully et al., 2019) (90% water by volume, with an overlying sublimation lag with a porosity of 0.5). Boxes indicate a plausible range of ages and VIR-derived grain sizes (Raponi et al., 2019).

eastern and western hemispheres differs by up to 4 wt.% (Figure 2b). Lower concentrations of hydrogen in the eastern hemisphere are consistent with LAMO observations (Prettyman et al., 2017); however, the high-resolution data reveal small scale variability, including enhanced concentrations of hydrogen in the Occator region (up to 2 wt.% eq. H_2O higher than surroundings). The northern hemisphere has more hydrogen than in the south and hydrogen at high latitudes increases more steeply in the north, perhaps indicating a larger gradient in ice table depth or ice concentration with latitude. The vertical lines that represent the statistical uncertainty in the data (Figure 2b) indicate these variations are significant.

A map of the distribution of hydrogen in the Occator region (Figure 2c) shows that Occator's interior and portions of the ejecta blanket to the east and south of the crater are richer in hydrogen than the surrounding low latitude region. Geologic mapping shows that Occator's ejecta blanket is asymmetrical, suggesting an oblique impact from the northwest (Scully et al., 2019). Relatively hydrogen-poor materials extend from the northern rim of the crater to the northeast, which partially overlaps a lane of dark ejecta shown in the geologic map (Figure 2c). Otherwise, the observed distribution of hydrogen is not closely aligned with geologic units.

4. Discussion

Hydrogen within Ceres' regolith is in the form of hydrated minerals, water ice, and other hydrogen-bearing species. Spectral mixing fractions were determined for a suite of detected minerals in the Occator region (Raponi et al., 2019). These included Mg-, Al-, and NH_4-bearing phyllosilicates, Mg- and Na-carbonates, NH_4-chloride, and a darkening agent. Following Marchi et al. (2019), the spectral mixing fractions were interpreted as volume fractions and combined with mineral densities and empirical formulae to estimate the concentration of hydrogen at Occator (Text S3). Both VIR and GRaND maps show a lobe of hydrogen-poor material extending to the northeast from the northern rim of the crater (Figure 3). Otherwise, they have dissimilar distributions and ranges, most likely due to differences in the hydration state of the regolith layers sensed by the instruments. VIR is sensitive to the uppermost ~100 μm surface layer; whereas, GRaND is sensitive to the uppermost meter. The presence of subsurface ice could account for the comparatively high dynamic range of GRaND data.

Outside the faculae, the VIR-derived hydrogen concentration spans 16–17 wt.% eq. H_2O, similar to the lowest values reported by GRaND (Figure 3a). Natrite (Na_2CO_3) is a significant component of the faculae (Raponi et al., 2019). It was suggested that Na-carbonates were initially hydrated (e.g., Zolotov, 2017); however, these hydrated species are not stable within the shallow subsurface within Occator crater (Text S4). As such, the faculae must be hydrogen poor (estimated to be about 10 wt.% eq. H_2O, ignoring bound water) compared to dark background materials. The faculae cover a small portion of the crater floor, well below the spatial scales resolved by GRaND even at closest approach (Figure S1). Consequently, hydrated salts are not likely a significant contributor to the hydrogen measured by GRaND within Occator crater.

Global variations in regolith hydrogen content, including the observed N-S and E-W differences (Figure 2), may not be caused by variations in the concentration of hydrated minerals. The dynamic range of VIR 2.7–3.1-μm band depths (OH and NH_4, respectively) is about one fifth that of subsurface hydrogen on the broad spatial scales sampled by GRaND in LAMO (Ammannito et al., 2016; Prettyman et al., 2019). Some variability in subsurface hydrogen may result from the presence of water bound to salts or interlayer water in clay minerals. However, detections of hydrated sodium carbonate are rare (Tosi et al., 2018) and if present may be in a low hydration state as nahcolite (Zolotov, 2017). Hydrated chloride salts, which could represent a significant crustal component depending on the freezing state of the ocean are not likely to be abundant in the shallow subsurface and regolith (Castillo-Rogez et al., 2018; De Sanctis et al., 2020).

Relatively high concentrations of hydrogen in the interior of Occator crater and its ejecta blanket probably result from the presence of subsurface water ice. Lobate deposits cover a significant portion (>30%) of the crater floor (Figure 2c) and may contain high concentrations of water ice (Scully et al., 2019). These likely formed following the impact by mixing of crustal water with rock to produce a water-rich slurry that filled portions of the crater's floor (Raponi et al., 2019; Scully et al., 2019). A portion of the excavated water would have been emplaced in the ejecta blanket (Schröder et al., 2021). As such, the heterogeneous distribution of hydrogen enhancements in and around Occator represent variations in the composition of materials ejected by the impact and their thermal history.

Thermophysical modeling shows that buried water ice, if present following impact, could still be found at depths sensed by GRaND in both the lobate deposits and the ejecta blanket, given Occator's age, assumed to be <20-Myr based on Neesemann et al. (2019), and a plausible range of regolith physical properties (Figure 3b). The rate at which ice retreats is controlled by the grain size and the porosity, which determine the vapor diffusion coefficient of the sublimation lag (Schorghofer, 2016; Text S4). When all other parameters are fixed, diffusivity increases with grain size. Based on data acquired by GRaND in LAMO, the global regolith has low porosity (0.2) and consists of fine grains (1 μm diameter) (Prettyman et al., 2017). The presence of μm-size particles is supported by spectrophotometry (Li et al., 2019); however, this contrasts with 10–100 μm grains derived from infrared observations (Gundlach & Blum, 2013; Raponi et al., 2019). Differences between grain size inferred for the surface and bulk regolith could result from interpretation of the data or physical processes, such as granular convection. The coarse grain sizes modeled in Figure 3b provide an upper limit on the expected ice depths.

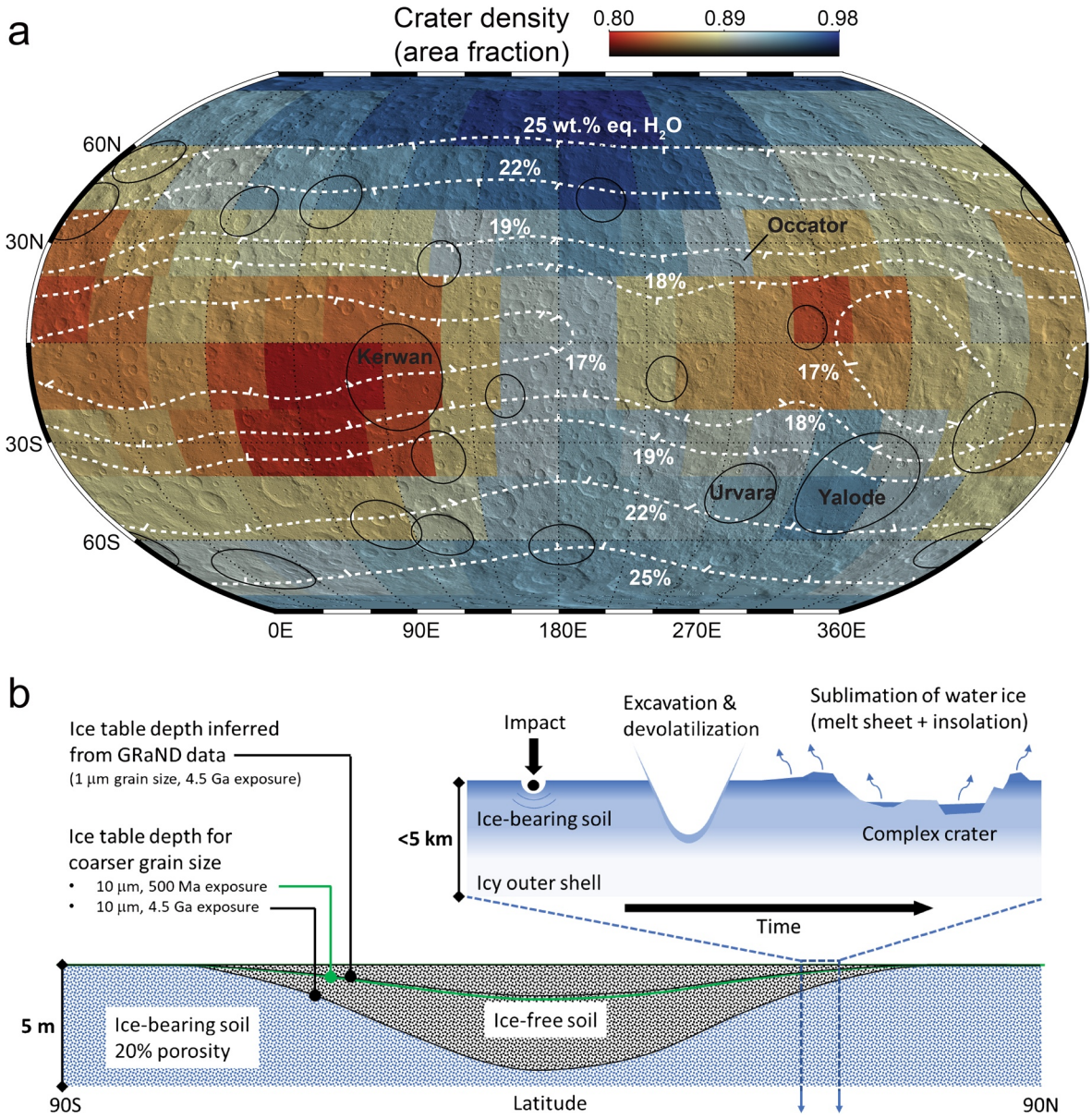

Figure 4. Impact processes as a partial control on the global distribution of hydrogen. (a) A map of the density of large craters is compared to the global distribution of hydrogen measured by the Gamma Ray and Neutron Detector (GRaND) (white contours). The map was determined by smoothing the pattern of large craters (20–100 km diameter) cataloged by Hiesinger et al. (2016) to the spatial resolution of GRaND in LAMO using the smoothing algorithm of Prettyman et al. (2019). A density of one indicates craters fully cover the surface within GRaND's field of view. For context, the map is superimposed on shaded relief and excluded basins with diameters greater than 100 km are outlined (black). Associations between crater density and the global distribution of hydrogen are detailed in Figures S2 and S3. (b) A possible scenario for enrichment of surficial ice by large impacts is illustrated. A portion of the ice excavated from the crust survives during crater formation and cooling of the melt sheet and ejecta blanket, enriching the regolith in water ice. The surviving ice retreats in response to solar insolation.

The global N-S asymmetry in hydrogen on Ceres suggests hemispheric differences in regolith ice content. This asymmetry cannot be explained by a receding ice table given Ceres' precessing orbital elements and reasonable models of surface roughness (Hayne & Aharonson, 2015; Landis et al., 2017; Prettyman et al., 2017; Schorghofer, 2016). Nevertheless, the detection of elevated hydrogen concentrations within and around Occator provides evidence for water ice emplaced in the regolith during the formation of large craters. Models predict that modification of the ice table by impact gardening is negligible (Costello et al., 2021; Schorghofer, 2016). We assess whether large impacts could influence the global distribution of hydrogen.

Hiesinger et al. (2016) cataloged craters greater than 20-diameter. Craters in the 20-100-km range sample the outer ∼2–10-km of the crust, a layer potentially rich in water ice (Park et al., 2020). The density of these craters when smoothed to the spatial resolution of GRaND exhibits a N-S asymmetry, like hydrogen, with highest density in the northern hemisphere (Figure 4a). In addition, elevated hydrogen concentrations extending from the northern to the southern hemisphere roughly corresponds with craters centered at 180°E (Figure S2). These associations suggest that the global distribution of hydrogen could be controlled—at least in part—by excavation of ice by large impacts; however, this hypothesis cannot fully explain the observed variability in hydrogen concentration (Figure S3). Impact basins excluded from the crater density map would have excavated deeper crustal materials perhaps with lower water content, modifying the composition of the regolith and crust in large portions of the eastern and southern hemisphere (e.g., Lawrence et al., 2018). Hidden basins (>280 km in diameter) would have dominated early regolith production and could also contribute to large-scale variations in the distribution of hydrogen (Marchi et al., 2016).

Hydrogen mapping data acquired by GRaND support shallow ice table depths, about 90 cm at the equator as illustrated in Figure 4b (Prettyman et al., 2017). The data are consistent with insolation-driven retreat over Ceres' 4.5 Gyr lifetime, assuming a fine-grained, low-diffusivity regolith. The ice depths inferred by GRaND can be explained if larger grain sizes are present, but only if the ice was emplaced more recently. For example, ice deposited ∼500 Myr ago would have retreated to 90 cm depth at the equator if the grain size were 10 μm. Consequently, delivery of crustal ice to the regolith by large impacts could influence the depth of near-surface ice. This would allow reconciliation of GRaND and VIR inferences of grain size.

5. Conclusions

Our analysis suggests the distribution of water ice within Ceres' bulk regolith is controlled by a combination of insolation-driven sublimation and delivery of water-bearing materials to the regolith from the volatile-rich outer crust by large impacts. The observed enrichment in hydrogen within Occator cater and ejecta blanket shows that excavated ice not only survives large impacts but also enhances the concentration of ice in the shallow subsurface. Associations between the pattern of large craters and the distribution of hydrogen suggest this process could be pervasive on Ceres. Impact replenishment of the regolith with crustal ice would allow the GRaND data to be explained by younger surface ages with larger regolith grain sizes more consistent with those inferred from infrared spectroscopy.

The high-resolution GRaND data support an endogenic crustal origin for ice within the regolith. Since the excavation depth of Occator was nearly 10 km, our results bring direct evidence for a large amount of ice in Ceres' crust, consistent with indirect inferences from geological observations (e.g., Sizemore et al., 2019). Alternative interpretations of the Dawn geophysical data in terms of an ice-free Ceres (Zolotov, 2020) are thus inconsistent with the GRaND data. The results also support the recent interpretation proposed by Schröder et al. (2021) for the distinctly blue color of ejecta from recent impact craters as an evolved mixture of ice and minerals.

Data Availability Statement

The Dawn Flight Team acquired the special, high-resolution data set used in this study. The GRaND data are available from the NASA Planetary Data System at https://sbn.psi.edu/pds/resource/dawn/dawngrand-PDS4.html.

Acknowledgments
Funding was provided by the NASA Discovery Data Analysis Program, the NASA SSERVI Toolkit for Research and Exploration project, and the NASA Dawn Mission. Part of this work was carried out at the Jet Propulsion Laboratory, California Institute of Technology, under contract to NASA. The authors thank B. L. Ehlmann for contributions to the interpretation of the data.

References

Ammannito, E., DeSanctis, M. C., Ciarniello, M., Frigeri, A., Carrozzo, F. G., Combe, J.-P., et al. (2016). Distribution of phyllosilicates on the surface of Ceres. *Science*, *353*(6303), aaf4279. https://doi.org/10.1126/science.aaf4279

Castillo-Rogez, J., Neveu, M., McSween, H. Y., Fu, R. R., Toplis, M. J., & Prettyman, T. (2018). Insights into Ceres's evolution from surface composition. *Meteoritics & Planetary Science*, *53*(9), 1820–1843. https://doi.org/10.1111/maps.13181

Combe, J.-P., Raponi, A., Tosi, F., De Sanctis, M. C., Carrozzo, F. G., Zambon, F., et al. (2019). Exposed H_2O-rich areas detected on Ceres with the dawn visible and infrared mapping spectrometer. *Icarus*, *318*, 22–41. https://doi.org/10.1016/j.icarus.2017.12.008

Costello, E. S., Ghent, R. R., & Lucey, P. G. (2021). Impact gardening on Ceres. *Geophysical Research Letters*, *48*, e2021GL092960. https://doi.org/10.1029/2021GL092960

De Sanctis, M. C., Ammannito, E., Raponi, A., Frigeri, A., Ferrari, M., Carrozzo, F. G., et al. (2020). Fresh emplacement of hydrated sodium chloride on Ceres from ascending salty fluids. *Nature Astronomy*, *4*(8), 786–793. https://doi.org/10.1038/s41550-020-1138-8

Ermakov, A. I., Fu, R. R., Castillo-Rogez, J. C., Raymond, C. A., Park, R. S., Preusker, F., et al. (2017). Constraints on Ceres' internal structure and evolution from its shape and gravity measured by the Dawn spacecraft. *Journal of Geophysical Research: Planets*, *122*(11), 2267–2293. https://doi.org/10.1002/2017je005302

Fu, R. R., Ermakov, A. I., Marchi, S., Castillo-Rogez, J. C., Raymond, C. A., Hager, B. H., et al. (2017). The interior structure of Ceres as revealed by surface topography. *Earth and Planetary Science Letters*, *476*, 153–164. https://doi.org/10.1016/j.epsl.2017.07.053

Gundlach, B., & Blum, J. (2013). A new method to determine the grain size of planetary regolith. *Icarus*, *223*(1), 479–492. https://doi.org/10.1016/j.icarus.2012.11.039

Hayne, P. O., & Aharonson, O. (2015). Thermal stability of ice on Ceres with rough topography. *Journal of Geophysical Research: Planets*, *120*(9), 1567–1584. https://doi.org/10.1002/2015je004887

Hiesinger, H., Marchi, S., Schmedemann, N., Schenk, P., Pasckert, J. H., Neesemann, A., et al. (2016). Cratering on Ceres: Implications for its crust and evolution. *Science*, *353*(6303). https://doi.org/10.1126/science.aaf4759

Landis, M. E., Byrne, S., Schörghofer, N., Schmidt, B. E., Hayne, P. O., Castillo-Rogez, J., et al. (2017). Conditions for sublimating water ice to supply Ceres' exosphere. *Journal of Geophysical Research: Planets*, *122*(10), 1984–1995. https://doi.org/10.1002/2017JE005335

Lawrence, D. J., Peplowski, P. N., Beck, A. W., Feldman, W. C., Prettyman, T. H., Russell, C. T., et al. (2018). Compositional variability on the surface of 1 Ceres revealed through GRaND measurements of high-energy gamma rays, *Meteoritics & Planetary Science 53*(9), 1805–1819. https://doi.org/10.1111/maps.13124

Li, J.-Y., Schröder, S. E., Mottola, S., Nathues, A., Castillo-Rogez, J. C., Schorghofer, N., et al. (2019). Spectrophotometric modeling and mapping of Ceres. *Icarus*, *322*, 144–167. https://doi.org/10.1016/j.icarus.2018.12.038

Marchi, S., Ermakov, A. I., Raymond, C. A., Fu, R. R., O'Brien, D. P., Bland, M. T., et al. (2016). The missing large impact craters on Ceres. *Nature Communications*, *7*, 12257. https://doi.org/10.1038/ncomms12257

Marchi, S., Raponi, A., Prettyman, T. H., De Sanctis, M. C., Castillo-Rogez, J., Raymond, C. A., et al. (2019). An aqueously altered carbon-rich Ceres. *Nature Astronomy*, *3*(2), 140–145. https://doi.org/10.1038/s41550-018-0656-0

McSween, H. Y., Emery, J. P., Rivkin, A. S., Toplis, M. J., Castillo-Rogez, C. J., Prettyman, T. H., et al. (2017). Carbonaceous chondrites as analogs for the composition and alteration of Ceres. *Meteoritics & Planetary Science*, *53*(8), 1793–1804. https://doi.org/10.1111/maps.12947

Neesemann, A., van Gasselt, S., Schmedemann, N., Marchi, S., Walter, S. H. G., Preusker, F., et al. (2019). The various ages of Occator crater, Ceres: Results of a comprehensive synthesis approach. *Icarus*, *320*, 60–82. https://doi.org/10.1016/j.icarus.2018.09.006

Park, R. S., Konopliv, A. S., Ermakov, A. I., Castillo-Rogez, J. C., Fu, R. R., Hughson, K. H. G., et al. (2020). Evidence of non-uniform crust of Ceres from Dawn's high-resolution gravity data. *Nature Astronomy*, *4*(8), 748–755. https://doi.org/10.1038/s41550-020-1019-1

Prettyman, T. H., Feldman, W. C., McSween, H. Y., Jr, Dingler, R. D., Enemark, D. C., Patrick, D. E., et al. (2011). Dawn's gamma ray and neutron detector. *Space Science Reviews*, *163*(1), 371–459. https://doi.org/10.1007/s11214-011-9862-0

Prettyman, T. H., Yamashita, N., Ammannito, E., Ehlmann, B. L., McSween, H. Y., Mittlefehldt, D. W., et al. (2019). Elemental composition and mineralogy of Vesta and Ceres: Distribution and origins of hydrogen-bearing species. *Icarus*, *318*, 42–55. https://doi.org/10.1016/j.icarus.2018.04.032

Prettyman, T. H., Yamashita, N., Toplis, M. J., McSween, H. Y., Schorghofer, N., Marchi, S., et al. (2017). Extensive water ice within Ceres' aqueously altered regolith: Evidence from nuclear spectroscopy. *Science*, *355*(6320), 55–59. https://doi.org/10.1126/science.aah6765

Quick, L. C., Buczkowski, D. L., Ruesch, O., Scully, J. E. C., Castillo-Rogez, J., Raymond, C. A., et al. (2019). A possible brine reservoir beneath Occator Crater: Thermal and compositional evolution and formation of the Cerealia dome and Vinalia Faculae. *Icarus*, *320*, 119–135. https://doi.org/10.1016/j.icarus.2018.07.016

Raponi, A., De Sanctis, M. C., Carrozzo, F. G., Ciarniello, M., Castillo-Rogez, J. C., Ammannito, E., et al. (2019). Mineralogy of Occator crater on Ceres and insight into its evolution from the properties of carbonates, phyllosilicates, and chlorides. *Icarus*, *320*, 83–96. https://doi.org/10.1016/j.icarus.2018.02.001

Raymond, C. A., Ermakov, A. I., Castillo-Rogez, J. C., Marchi, S., Johnson, B. C., Hesse, M. A., et al. (2020). Impact-driven mobilization of deep crustal brines on dwarf planet Ceres. *Nature Astronomy*, *4*(8), 741–747. https://doi.org/10.1038/s41550-020-1168-2

Ruesch, O., Genova, A., Neumann, W., Quick, L. C., Castillo-Rogez, J. C., Raymond, C. A., et al. (2019). Slurry extrusion on Ceres from a convective mud-bearing mantle. *Nature Geoscience*, *12*(7), 505–509. https://doi.org/10.1038/s41561-019-0378-7

Russell, C. T., Raymond, C. A., Ammannito, E., Buczkowski, D. L., De Sanctis, M. C., Hiesinger, H., et al. (2016). Dawn arrives at Ceres: Exploration of a small, volatile-rich world. *Science*, *353*(6303), 1008–1010. https://doi.org/10.1126/science.aaf4219

Schenk, P., Castillo-Rogez, J., Otto, K. A., Marchi, S., O'Brien, D., Bland, M., et al. (2021). Compositional control on impact crater formation on mid-sized planetary bodies: Dawn at Ceres and Vesta, Cassini at Saturn. *Icarus*, *359*, 114343. https://doi.org/10.1016/j.icarus.2021.114343

Schorghofer, N. (2016). Predictions of depth-to-ice on asteroids based on an asynchronous model of temperature, impact stirring, and ice loss. *Icarus*, *276*, 88–95. https://doi.org/10.1016/j.icarus.2016.04.037

Schröder, S. E., Poch, O., Ferrari, M., Angelis, S. D., Sultana, R., Potin, S. M., et al. (2021). Dwarf planet (1) Ceres surface bluing due to high porosity resulting from sublimation. *Nature Communications*, *12*(1), 274. https://doi.org/10.1038/s41467-020-20494-5

Scully, J. E. C., Buczkowski, D. L., Raymond, C. A., Bowling, T., Williams, D. A., Neesemann, A., et al. (2019). Ceres' Occator crater and its faculae explored through geologic mapping. *Icarus*, *320*, 7–23. https://doi.org/10.1016/j.icarus.2018.04.014

Sizemore, H. G., Platz, T., Schorghofer, N., Prettyman, T. H., De Sanctis, M. C., Crown, D. A., et al. (2017). Pitted terrains on (1) Ceres and implications for shallow subsurface volatile distribution. *Geophysical Research Letters*, *44*(13), 6570–6578. https://doi.org/10.1002/2017GL073970

Sizemore, H. G., Schmidt, B. E., Buczkowski, D. A., Sori, M. M., Castillo-Rogez, J. C., Berman, D. C., et al. (2019). A global inventory of ice-related morphological features on dwarf planet Ceres: Implications for the evolution and current state of the cryosphere. *Journal of Geophysical Research: Planets*, *124*, 1650–1689. https://doi.org/10.1029/2018JE005699

Tosi, F., Carrozzo, F. G., Raponi, A., De Sanctis, M. C., Thangjam, G., Zambon, F., et al. (2018). Mineralogy and temperature of crater Haulani on Ceres. *Meteoritics & Planetary Science*, *53*(9), 1902–1924. https://doi.org/10.1111/maps.13078

Williams, D. A., Buczkowski, D. L., Crown, D. A., Frigeri, A., Hughson, K., Kneissl, T., et al. (2019). *Final Dawn LAMO-based global geologic map of Ceres*. Conference: 50th Lunar and Planetary Science. https://www.hou.usra.edu/meetings/lpsc2019/pdf/1252.pdf

Williams, D. A., Buczkowski, D. L., Mest, S. C., Scully, J. E. C., Platz, T., & Kneissl, T. (2018). Introduction: The geologic mapping of Ceres. *Icarus*, *316*, 1–13. https://doi.org/10.1016/j.icarus.2017.05.004

Zolotov, M. Y. (2017). Aqueous origins of bright salt deposits on Ceres. *Icarus*, *296*, 289–304. https://doi.org/10.1016/j.icarus.2017.06.018

Zolotov, M. Y. (2020). The composition and structure of Ceres' interior. *Icarus*, *335*, 113404. https://doi.org/10.1016/j.icarus.2019.113404

References From the Supporting Information

Bu, C., Rodriguez Lopez, G., Dukes, C. A., McFadden, L. A., Li, J. Y., & Ruesch, O. (2018a). Stability of hydrated carbonates on Ceres. *Icarus*, *320*, 136–149. https://doi.org/10.1016/j.icarus.2017.12.036

Bu, C., Rodriguez Lopez, G., Dukes, C. A., Ruesch, O., McFadden, L. A., & Li, J. Y. (2018b). Search for sulfates on the surface of Ceres. *Meteoritics & Planetary Science*, *53*(9), 1946–1960. https://doi.org/10.1111/maps.13024

Carrozzo, F. G., De Sanctis, M. C., Raponi, A., Ammannito, E., Castillo-Rogez, J., Ehlmann, B. L., et al. (2018). Nature, formation, and distribution of carbonates on Ceres. *Science Advances*, *4*(3), e1701645. https://doi.org/10.1126/sciadv.1701645

De Sanctis, M. C., Ammannito, E., Raponi, A., Marchi, S., McCord, T. B., McSween, H. Y., et al. (2015). Ammoniated phyllosilicates with a likely outer Solar System origin on (1) Ceres. *Nature*, *528*(7581), 241–244. https://doi.org/10.1038/nature16172

Haines, E. L., Etchegaray-Ramirez, M. I., & Metzger, A. E. (1978). Thorium concentrations in the lunar surface. II: Deconvolution modeling and its application to the regions of Aristarchus and Mare Smythii. *Proceedings of the Lunar and Planetary Science Conference*, *9*, 2985–3013.

Landis, M. E., Byrne, S., Combe, J.-P., Marchi, S., Castillo-Rogez, J., Sizemore, H. G., et al. (2019). Water vapor contribution to Ceres' exosphere from observed surface ice and postulated ice-exposing impacts. *Journal of Geophysical Research: Planets*, *124*(1), 61–75. https://doi.org/10.1029/2018je005780

Lawrence, D., Elphic, R., Feldman, W., Prettyman, T., Gasnault, O., & Maurice, S. (2003). Small-area thorium features on the lunar surface. *Journal of Geophysical Research*, *108*(E9), 5102. https://doi.org/10.1029/2003je002050

Li, J.-Y., Reddy, V., Nathues, A., Corre, L. L., Izawa, M. R. M., Cloutis, E. A., et al. (2016). Surface albedo and spectral variability of Ceres. *The Astrophysical Journal*, *817*(2), L22. https://doi.org/10.3847/2041-8205/817/2/l22

Maurice, S., Lawrence, D. J., Feldman, W. C., Elphic, R. C., & Gasnault, O. (2004). Reduction of neutron data from Lunar Prospector. *Journal of Geophysical Research*, *109*(E7). https://doi.org/10.1029/2003JE002208

McCord, T. B., Orlando, T. M., Teeter, G., Hansen, G. B., Sieger, M. T., Petrik, N. G., & Van Keulen, L. (2001). Thermal and radiation stability of the hydrated salt minerals epsomite, mirabilite, and natron under Europa environmental conditions. *Journal of Geophysical Research*, *106*(E2), 3311–3319. https://doi.org/10.1029/2000JE001282

McKinney, G. W., Lawrence, D. J., Prettyman, T. H., Elphic, R. C., Feldman, W. C., & Hagerty, J. J. (2006). MCNPX benchmark for cosmic ray interactions with the Moon. *Journal of Geophysical Research*, *111*(E6), E06004. https://doi.org/10.1029/2005je002551

Park, R. S., & Buccino, D. R. (2018). *Ceres SPC shape model dataset V1.0, DAWN-A-FC2-5-CERESSHAPESPC-V1.0. NASA planetary data System*.

Park, R. S., Vaughan, A. T., Konopliv, A. S., Ermakov, A. I., Mastrodemos, N., Castillo-Rogez, J. C., et al. (2019). High-resolution shape model of Ceres from stereophotoclinometry using Dawn Imaging Data. *Icarus*, *319*, 812–827. https://doi.org/10.1016/j.icarus.2018.10.024

Prettyman, T. H., Feldman, W. C., & Titus, T. N. (2009). Characterization of Mars' seasonal caps using neutron spectroscopy. *Journal of Geophysical Research*, *114*(E8). https://doi.org/10.1029/2008je003275

Prettyman, T. H., Mittlefehldt, D. W., Yamashita, N., Lawrence, D. J., Beck, A. W., Feldman, W. C., et al. (2012). Elemental mapping by Dawn reveals exogenic H in Vesta's regolith. *Science*, *338*(6104), 242–246. https://doi.org/10.1126/science.1225354

Rivkin, A. S., Li, J.-Y., Milliken, R. E., Lim, L. F., Lovell, A. J., Schmidt, B. E., et al. (2011). The surface composition of Ceres. *Space Science Reviews*, *163*(1–4), 95–116. https://doi.org/10.1007/s11214-010-9677-4

Schorghofer, N. (2008). The lifetime of ice on main belt asteroids. *The Astrophysical Journal*, *682*(1), 697–705. https://doi.org/10.1086/588633